Orbital mismatch boosting nematic instability in iron-based superconductors

Orbital mismatch boosting nematic instability in iron-based superconductors

Laura Fanfarillo,[1] Lara Benfatto,[2,*] and Belén Valenzuela[3,†]

[1] *CNR-IOM and International School for Advanced Studies (SISSA), Via Bonomea 265, I-34136, Trieste, Italy*
[2] *ISC-CNR and Dep. of Physics, "Sapienza" University of Rome, P.le A. Moro 5, 00185, Rome, Italy*
[3] *Instituto de Ciencia de Materiales de Madrid, ICMM-CSIC, Cantoblanco, E-28049 Madrid, Spain*

(Dated: July 26, 2018)

We derive the effective action for the collective spin modes in iron-based superconductors. We show that, due to the orbital-selective nature of spin fluctuations, the magnetic and nematic instabilities are controlled by the degrees of orbital nesting between electron and hole pockets. Within a prototypical three-pockets model the hole-electron orbital mismatch is found to boost spin-nematic order. This explains the enhancement of nematic order in FeSe as compared to 122 compounds, and its suppression under pressure, where the emergence of the second hole pocket compensates the orbital mismatch of the three-pockets configuration.

PACS numbers: 74.70.Xa, 74.25.nd

Understanding the origin of the nematic phase is one of the most challenging open issues in the field of iron-based superconductors (IBS). In these systems the structural transition from tetragonal to orthorhombic is accompanied (and often preempted) by a marked electronic anisotropy which suggests an electronic origin of the instability [1]. The original spin-nematic proposal [2, 3] focuses on the typical topology of the Fermi surface (FS) in pnictides, with hole-(h-)like pockets at Γ and electron-(e-)like pockets at $\mathbf{Q}_X = (\pi, 0)$ and $\mathbf{Q}_Y = (0, \pi)$ in the 1Fe unit-cell notation. The underlying idea is that the nesting between h- and e-pockets favors the spin fluctuations at these two equivalent momenta. According to [2, 3], a nematic phase emerges since the ellipticity of the e-pockets induces an anisotropy of the paramagnetic spin fluctuations before that the long-range magnetic order sets in, lowering the symmetry of the electronic response from C_4 to C_2. This appealing scenario is however challenged by the fact that nematicity is observed to be stronger or weaker in systems with similar band structure.

FeSe is a remarkable example. Here the undoped compound has a structural transition at $T_S = 90K$ which is only cut-off below by the superconducting transition at $T_c = 9K$ [4]. The lack of magnetic order motivated alternative interpretations for nematicity as due to orbital ordering [5–10]. On the other hand, sizeable spin fluctuations have been detected in FeSe as well [11, 12], triggering an intense investigation on the interplay between spin and orbital degrees of freedom[10, 13–18]. Despite some interesting proposals [19–21], no consensus has been reached yet on the mechanism favouring nematicity in FeSe as compared to other systems, and leading to its suppression with external and internal pressure [22–24].

In this Rapid Communication we show that the spin-nematic scenario is able to discriminate topologically equivalent band structures once that the original derivation [2, 3] is crucially revised accounting for the orbital character of the bands. On general grounds, the importance of the orbital content of the FS for the low-energy spin-fluctuations in IBS, pointed out in [13], has been recently discussed within several contexts [18, 25–27]. Here we show that the orbital topology of the FS crucially affects the spin-nematic instability itself, which is controlled by the degree of orbital nesting, i.e. the relative orbital composition between the h- and e-pockets involved in the spin-exchange mechanism. By projecting the general microscopic interaction[28–32] on the low-energy multiorbital model of [33] spin fluctuations at dif-

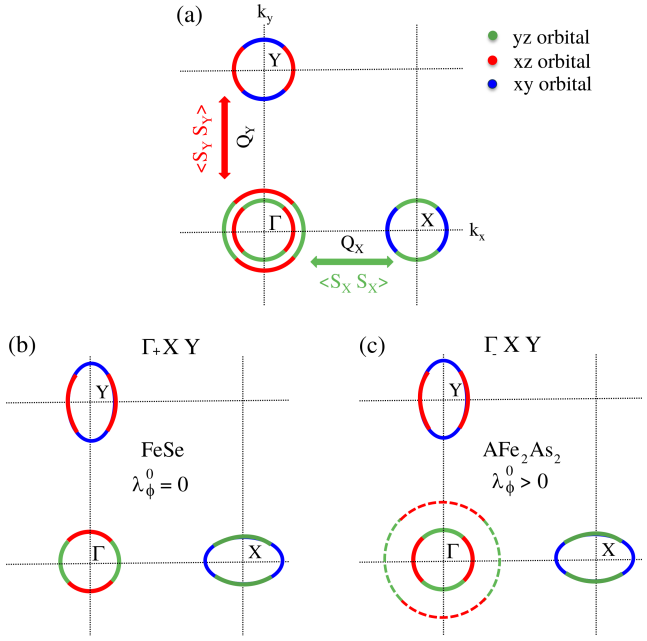

FIG. 1: (a) General sketch of the orbital content of the FS of 4-pocket model for IBS. The green/red arrows denote the OSSF, connecting h- and e-pockets at different momenta. (b) Sketch of FeSe: only the outer pocket is present. (c) Sketch of 122 systems: the outer pocket is much larger, so it can be neglected in first approximation. The orbital mismatch (matching) in panel b (c) is determined by the out-of-phase (in-phase) angular dependence of the yz/xz orbital in the h- and X/Y e-pockets.

ferent $\mathbf{Q}$ vectors become orbital selective, i.e. they involve only specific orbitals [13], see Fig. 1a. As a result also the interactions between spin modes beyond Gaussian level, responsible for the nematic instability, becomes renormalized by the orbital content of the h- and e-pockets. In particular we find that orbital nesting can differentiate two topologically equivalent three-pocket models in which a single hole pocket is present at Γ. In the case of FeSe the relevant h-pocket is the outer one, see Fig. 1b, and we find that its orbital mismatch with the e-pockets boosts the nematic instability, while it is detrimental for magnetism. In contrast, in the 122 family the most relevant h-pocket is the inner one [34–36], having opposite orbital character, see Fig. 1b. In this case its good orbital nesting with the e-pockets explains the robustness of the magnetic phase and the appearance of a nematic instability only in its proximity. Along the same reasoning, we argue that in FeSe the suppression of nematicity with internal or external pressure [22–24] can be ascribed to the emergence of the inner hole pocket, changing the FS orbital topology towards a more symmetric four-pocket model where nematicity can be easily lost.

We consider first a general four-pocket model with two h-pockets at Γ, $\Gamma_\pm$ and two e-pockets at X and Y, that can be easily adapted to describe different compounds among the 122 and 11 families. The kinetic part of the Hamiltonian is derived adapting the low-energy model considered in [33], where each pocket is described using a spinor representation in the pseudo-orbital space [18, 33]

$$H_0^l = \sum_{\mathbf{k},\sigma} \psi^{l,\dagger}_{\mathbf{k}\sigma} \hat{H}^l_0 \psi^l_{\mathbf{k}\sigma}, \tag{1}$$

with $\hat{H}^l_0 = h^l_0\tau_0 + \vec{h}^l\cdot\vec{\tau}$, $l = \Gamma, X, Y$ and τ matrices represent the pseudo-orbital spin. The spinors are defined as $\psi^\Gamma = (c_{yz}, c_{xz})$ and $\psi^{X/Y} = (c_{yz/xz}, c_{xy})$. Diagonalizing $\hat{H}_0$ we find the dispersion relations $E^{l\pm} = h^l_0 \pm h^l$ with $h^l = |\vec{h}^l|$. We introduce the rotation from the orbital to the band basis,

$$\begin{pmatrix} h_+ \\ h_- \end{pmatrix} = \begin{pmatrix} u_\Gamma & -v_\Gamma \\ v_\Gamma & u_\Gamma \end{pmatrix} \begin{pmatrix} c_{yz} \\ c_{xz} \end{pmatrix} \tag{2}$$

with an analogous expression for the X/Y pockets, provided that the corresponding orbital spinor is used. At X/Y only the $E^{X/Y+}$ band crosses the Fermi level, so in the following we will use $e_{X/Y}$ for the corresponding fermonic operators dropping the + subscript.

The interacting Hamiltonian is given by

$$H_{int} = -1/2 \sum_{\mathbf{q}\,'} U_{\eta\eta'} \vec{S}^\eta_{\mathbf{q}} \cdot \vec{S}^{\eta'}_{-\mathbf{q}}. \tag{3}$$

with $\eta, \eta' = yz, xz, xy$ denoting the orbital index. The interaction in the spin channel is defined as $U_{\eta\eta'} \sim U\delta_{\eta\eta'} + J_H(1-\delta_{\eta\eta'})$, U and J_H being the usual Hubbard and Hund couplings. We consider only spin operators with intraorbital character $\vec{S}^\eta_{\mathbf{q}} = \sum_{\mathbf{k}ss'} (c^{\eta\dagger}_{\mathbf{k}s} \vec{\sigma}_{ss'} c^\eta_{\mathbf{k}+\mathbf{q}s'})$ with $\sigma_{ss'}$ are the Pauli matrices for the spin operator. This choice is motivated by the general finding that intraorbital magnetism is the dominant channel in IBS [28–32]. The relevant magnetic fluctuations occur at momenta $\mathbf{q}$ near $\mathbf{Q}_X$ or $\mathbf{Q}_Y$. At low energy we can project out the general interaction, Eq. (3), onto the fermionic excitations defined by the model (1). By using the rotation to the band basis, Eq. (2), one can then establish a precise correspondence between the orbital and momentum character of the spin operators $\vec{S}^\eta_{X/Y} \equiv \vec{S}^\eta_{\mathbf{q}=\mathbf{Q}_{X/Y}}$:

$$\vec{S}^{yz}_X = \sum_{\mathbf{k}} (u_\Gamma h^\dagger_+ + v_\Gamma h^\dagger_-)\, \vec{\sigma}\, u_X e_X \tag{4}$$

$$\vec{S}^{xz}_Y = \sum_{\mathbf{k}} (-v_\Gamma h^\dagger_+ + u_\Gamma h^\dagger_-)\, \vec{\sigma}\, u_Y e_Y \tag{5}$$

where we drop for simplicity the momentum and spin indices of the fermionic operators. It then follows that the interacting Hamiltonian Eq.(3) reduces to

$$H_{int} = -\frac{\tilde{U}}{2} \sum_{\mathbf{q}\,'} \vec{S}^{yz/xz}_{X/Y} \cdot \vec{S}^{yz/xz}_{X/Y}. \tag{6}$$

where $\tilde{U}$ is the intraorbital interaction renormalized at low energy. As it is clear from the above equation, it is the projection of the generic interaction Hamiltonian (3) onto the low-energy model (1) that generates orbital-selective spin fluctuations (OSSF). Indeed, since at low energy the xz/yz-fermionic states exist only around Q_Y/Q_X, it turns out that the spin operators $\vec{S}^\eta_X$ with $\eta \neq yz$ and $\vec{S}^\eta_Y$ with $\eta \neq xz$ are absent in Eq. (6), so that there are no terms involving the Hund's coupling. Once this correspondence has been establihed the derivation of the effective action is formally equivalent to the one used in the simplified band language [2]. One can decouple the interaction term, Eq. (3), by means of two vectorial Hubbard-Stratonovich (HS) fields $\vec{\Delta}^{yz/xz}_{X/Y}$ which will describe in what follows the collective electronic spin fluctuations. The effective action up to quartic order becomes:

$$\begin{aligned} S_{\text{eff}} &= \begin{pmatrix} \Delta^{yz}_X & \Delta^{xz}_Y \end{pmatrix} \begin{pmatrix} \chi^{-1}_X & 0 \\ 0 & \chi^{-1}_Y \end{pmatrix} \begin{pmatrix} \Delta^{yz}_X \\ \Delta^{xz}_Y \end{pmatrix} \\ &+ \begin{pmatrix} (\Delta^{yz}_X)^2 & (\Delta^{xz}_Y)^2 \end{pmatrix} \begin{pmatrix} u_{11} & u_{12} \\ u_{12} & u_{22} \end{pmatrix} \begin{pmatrix} (\Delta^{yz}_X)^2 \\ (\Delta^{xz}_Y)^2 \end{pmatrix} \end{aligned} \tag{7}$$

Here $\chi^{-1}_{X/Y} = 1/U_s + \Pi^{yz/xz}_{X/Y}$, where U_s is the effective interactions between low-energy quasiparticles, and $\Pi^{yz/xz}_{X/Y}$ is the propagator in the long-wavelength and zero-frequency limit:

$$\Pi^{yz}_X = T \sum_{\mathbf{k}, i\omega_n} u^2_\Gamma u^2_X g_+ g_X + v^2_\Gamma u^2_X g_- g_X, \tag{8}$$

$$\Pi^{xz}_Y = T \sum_{\mathbf{k}, i\omega_n} v^2_\Gamma u^2_Y g_+ g_Y + u^2_\Gamma u^2_Y g_- g_Y. \tag{9}$$

$g_i(\mathbf{k}, i\omega_n) = (i\omega_n - E^i_{\mathbf{k}})^{-1}$ are the Green's functions in the band basis, $i = \pm$ denotes the h-bands and $i = X, Y$ the electronic ones. The coefficients of the quartic part of the action in Eq.(7) are (see also [26]):

$$u_{11} = T \sum_{\mathbf{k}, i\omega_n} (u_X^2 g_X)^2 (u_\Gamma^2 g_+ + v_\Gamma^2 g_-)^2, \quad (10)$$

$$u_{22} = T \sum_{\mathbf{k}, i\omega_n} (u_Y^2 g_Y)^2 (v_\Gamma^2 g_+ + u_\Gamma^2 g_-)^2, \quad (11)$$

$$u_{12} = T \sum_{\mathbf{k}, i\omega_n} u_X^2 g_X u_Y^2 g_Y u_\Gamma^2 v_\Gamma^2 (g_+ - g_-)^2. \quad (12)$$

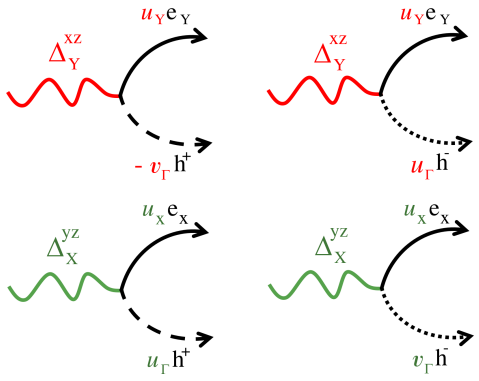

FIG. 2: Diagrammatic representation of the vertices connecting the HS fields to the fermionic operators. Wavy (red/green) line denote the HS fields ($\Delta^{yz/xz}_{X/Y}$), solid lines the excitations in the e-pockets, dashes/dotted lines excitations in the outer/inner h-pocket. The u_l, v_l coefficients account for the orbital component of each band, according to the low-energy projection (4)-(5).

As usual, the effective action is an expansion in powers of the HS fields. The coefficients of the n^{th} power of the field is a loop with n fermionic lines, leading to the product of two or four Green's functions in Eq. (8)-(9) and (10)-(12), respectively. The vertices connecting $\Delta^{yz/xz}_{X/Y}$ to the band operators are depicted in Fig. (2). Using this correspondence, which follows from the projection (4)-(5) of the spin operators at low energy, one easily understands that the fermionic loops are weighted with the elements u_l, v_l defining the orbital content of each band. The magnetic instability is controlled by the Gaussian part of the action, Eq. (7), and it occurs at the temperature where the inverse $Q_{X/Y}$ susceptibilities $\chi^{-1}_{X/Y}$ vanish. The nematic instability happens when the fluctuations along the x and y directions become inequivalent already above T_N. Since $u_{11} = u_{22}$ due to C_4 symmetry, the quartic part of the action, Eq. (7) can be simply diagonalized as

$$S^{(4)}_{\text{eff}} = \lambda_\psi \psi^2 + \lambda_\phi \phi^2 \quad (13)$$

where

$$\psi = \frac{1}{\sqrt{2}} \left((\Delta_X^{yz})^2 + (\Delta_Y^{xz}) \right)^2, \quad \lambda_\psi = u_{11} + u_{12} \quad (14)$$

$$\phi = \frac{1}{\sqrt{2}} \left((\Delta_X^{yz})^2 - (\Delta_Y^{xz}) \right)^2, \quad \lambda_\phi = u_{11} - u_{12}. \quad (15)$$

Notice that the tensorial form of the nematic order parameter proposed in Ref. [14] does not contain our result Eq. (24), which in turn is dictated by the only possible non-Gaussian terms Eq. (7) for the OSSF. From Eq. (13) one sees that a nematic instability is possible only for $\lambda_\phi < 0$, when making $\langle \phi \rangle \neq 0$ lowers the energy of the system. However, while in Ref. [2] λ_ϕ is only controlled by the shape of the e-pockets, we find that also the degree of orbital nesting plays an important role.

To make a first estimate of this effect we consider the simple case where the e-/h-pockets are perfectly nested circular FS, so that the orbital weights reduce to, $u_\Gamma = u_Y = v_X = \cos\theta_{\mathbf{k}}$, $v_\Gamma = v_Y = u_X = \sin\theta_{\mathbf{k}}$ and the Green's functions can be written as $g_X = g_Y = g_e = (i\omega_n - \epsilon)^{-1}$, $g_+ = g_- = g_h = (i\omega_n + \epsilon)^{-1}$, with $\epsilon = -\epsilon_0 + \mathbf{k}^2/2m - \mu$. ϵ_0 is the off-set energy, m the parabolic band mass and μ the chemical potential. Within this approximation we can carry out explicitly the integration in Eq.s (8)-(12), showing that the differences between the various terms arise only from the angular integration of the product of the orbital weights. For what concerns the magnetic instability, the spin-fluctuations bubbles $\Pi^{yz/xz}_{X/Y}$, Eq.s (8)-(9), are both proportional to $\Pi_{eh} = T \sum_{\mathbf{k}, i\omega_n} g_e g_h$ that lead to the usual log divergence: $\Pi_{eh} \sim -N_F \log \omega_0/T$ where N_F is the density of states and ω_0 an upper cut-off [37]. On the other hand, the orbital renormalization of the $S^{(4)}_{\text{eff}}$ action is much more severe. Indeed, considering two hole pockets of same size, one immediately finds from Eq. (12) that $u_{12} = 0$. This leads to a large *positive* nematic eigenvalue λ_ϕ in Eq. (24), which prevents the occurrence of nematicity, in agreement with recent renormalization group studies on the 4-pocket model [27].

To simulate the case of specific compounds we consider two 3-pocket models in which a single hole pocket at Γ is well-nested with the elliptical e-pockets: (a) The $3p_+$ model for FeSe (Fig. 1b), where only the outer pocket Γ_+ crosses the Fermi level while the inner pocket Γ_- sinks below it before the nematic transition [18, 24]; (b) The $3p_-$ model for 122 systems (Fig. 1c), where the outer pocket Γ_+ is much larger than the electron ones, so it weakly contributes to the nesting [38, 39]. These two models would be equivalent within the simplified band approach [2] but lead to different OSSF actions. As far as nematicity is concerned, we see that while the u_{12} term in Eq. (12) is the same when only one of the two hole pockets is considered, the u_{11} and u_{22} terms pick up in a different way the orbital weights at Γ, allowing us to discriminate between the two cases.

(a) FeSe: As it has been recently discussed in [18], the disappearance of the inner hole pocket in FeSe can be explained by the combined effect of spin-orbit coupling and OSSF shrinking mechanism. When only the Γ_+ pocket is considered in Eq.s (10)-(12) all the coefficients of the quartic action become equal, so that at leading order $\lambda_\psi^0 > 0$ and $\lambda_\phi^0 = 0$. Following the same lines of [2], we then include at perturbative level the e-pockets ellipticity and the deviations from perfect nesting. Since the results are robust with respect to the latter perturbation [37], we discuss here only the dependence on the ellipticity parameter δ_e. In this case, the eigenvalues of the quartic action turn out to be:

$$\lambda_\psi^{3p_+} = 3\mathcal{K}(T), \qquad \lambda_\phi^{3p_+} = -\mathcal{K}(T)\frac{b\,\delta_e^2}{T^2} \tag{16}$$

with $\mathcal{K}(T) = 7N_F\zeta(3)/(8^3\pi^2T^2)$. As one can see, as soon as a finite ellipticity is included, $\lambda_\phi < 0$ at any temperature. This result is then analogous to the one found in the simplified band language of Ref. [2], and the nematic critical temperature is determined by the divergence of the full nematic susceptibility $\chi_{nem} = \int_q \chi_X^2/(1+\lambda_\phi \int_q \chi_X^2)$ [40]. On the other hand, the orbital mismatch between the h- and e-pockets realized in the case of FeSe is detrimental for the magnetic instability itself. Indeed, when only the Γ_+ pocket is present the magnetic propagator in Eq. (8)-(9) is reduced by a factor 1/8 with respect to Π_{eh} found in the simplified band language, since $\Pi_{X/Y}^{yz/xz} \sim \Pi_{eh}\int(d\theta/2\pi)\cos^2\theta\sin^2\theta = \Pi_{eh}/8$ [37].

(b) 122 systems: In this case the good orbital nesting between the h- and e- pockets makes the u_{11} term (10) much larger than the u_{12} term (12), so that at leading order λ_ϕ^0 in Eq. (24) is *positive*, preventing a nematic transition. Accounting for the ellipticity of the e-pockets one finds:

$$\lambda_\psi^{3p_-} = \mathcal{K}(T)\left(19-\frac{12\,b\,\delta_e^2}{T^2}\right),\ \lambda_\phi^{3p_-} = \mathcal{K}(T)\left(16-\frac{25}{2}\frac{b\,\delta_e^2}{T^2}\right), \tag{17}$$

so that the ellipticity is again the driving force for the nematic transition. However in this case $\lambda_\phi^{3p_-}$ (which always becomes negative first) changes sign only below a temperature T^* scaling as $T^* \sim 0.19\,\delta_e$ [37]. At the same time the good orbital nesting pushes the magnetic transition to higher temperatures, since $\Pi_{X/Y}^{yz/xz} \sim 3\Pi_{eh}/8$.

To make a quantitative comparison between the two 3pockets models we show in Fig. 3 a-b the magnetic susceptibility $\chi_{X/Y}^{yz/xz}$(q=0) and the nematic eigenvalue λ_ϕ using the same set of band parameters, as appropriate e.g. for 122 compounds [37]. As one can see, by accounting uniquely for the different orbital nesting the Neél temperature of the $3p_+$ model, $T_{Neel}^{3p_+}$, is suppressed by about 80% with respect to the $3p_-$ case. Taking into account also that the experimental density of states in FeSe is smaller than in 122 compounds [18] $T_{Neel}^{3p_+}$ is expected to be further suppressed [37]. Finally from Fig. 3b, one observes that while $\lambda_\phi^{3p_+}$ is always negative, $\lambda_\phi^{3p_-}$ changes sign slightly above the $T_{Neel}^{3p_-}$, and then rapidly increases in absolute value. These considerations provides a possible explanation of the observed proximity between the nematic and magnetic transition in 122 systems [41].

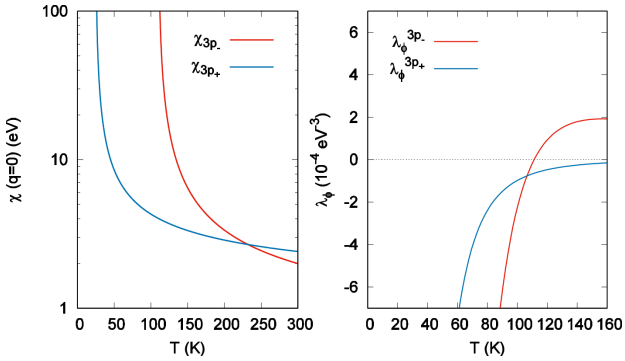

FIG. 3: (a)$\chi_{X/Y}^{yz/xz}$(q=0) and (b) nematic eigenvalue λ_ϕ for the $3p_+$ and $3p_-$ model for the same set of band parameters (see text). Here $T_{Neel} = 110$, 24 K for the $3p_-$, $3p_+$ model respectively, while the change of sign of λ_ϕ for the $3p_-$ model occurs around 112 K.

The above results offers also a possible explanation for the suppression of nematicity in FeSe under internal and external pressure. Indeed, it has been reported that Sulphur isoelectronic substitution [24, 42] brings back the inner hole pocket above the Fermi level. This finding is also supported by ab-initio calculations, which usually miss the experimental position of the Fermi level but report in general an increase of the hole-pockets size with pressure [21, 43]. The emergence of the inner hole pocket changes the FS topology of FeSe towards the more symmetric 4-pocket model, which has been shown before to be detrimental for nematicity, leading to the largest positive value of the λ_ϕ^0 eigenvalue. On the other hand, the same mechanism could also enhance magnetism, as observed. How these two effects interplay with the concomitant increase of the superconductivity remains an open question for future studies.

In conclusion, we derived the effective model for the spin fluctuations starting from a multiorbital low-energy 4-pockets fermionic model. We showed that orbital degrees of freedom renormalize the effective interactions between spin modes, with observable consequences on the magnetic and nematic instabilities. We considered explicitly a prototype 3-pockets model, as appropriate for FeSe and 122 compounds, where the only difference between the two cases is the orbital content of the relevant h-pocket at Γ. In FeSe the orbital mismatch between the outer h-pocket and the electron ones boosts nematicity and is detrimental for magnetism. In 122 compounds the good h-e orbital nesting favors magnetism and makes nematicity possible only at temperatures close to the magnetic transition. Our results offers a unified scenario to

understand how orbital nesting can differentiate topologically equivalent band structures. Further confirmations of this mechanism can provide an useful tool to ultimately reach the external control on nematic order in iron-based systems.

Acknowledgment

L.F. and B.V. acknowledges Jörg Fink for useful discussions. B.V. acknowledges Roser Valenti for discussion and for sharing her ab-initio calculations of FeSe with pressure. L.B. acknowledges financial support by Italian MIUR under project PRIN-RIDEIRON-2012X3YFZ2 and by MAECI under the Italian-India collaborative project SUPERTOP-PGR04879. B.V. acknowledges funding from MINECO (Spain) via Grants No.FIS2014-53219-P and Fundación Ramón Areces.

* corresponding author: lara.benfatto@roma1.infn.it
† corresponding author: belenv@icmm.csic.es

[1] Y. Gallais and I. Paul, Comptes Rendus Physique **17**, 113 (2016).
[2] R. M. Fernandes, A. V. Chubukov, J. Knolle, I. Eremin, and J. Schmalian, Phys. Rev. B **85**, 024534 (2012).
[3] R. M. Fernandes, A. V. Chubukov, and J. Schmalian, Nat Phys **10**, 97 (2014).
[4] A. E. Böhmer, F. Hardy, F. Eilers, D. Ernst, P. Adelmann, P. Schweiss, T. Wolf, and C. Meingast, Phys. Rev. B **87**, 180505 (2013).
[5] S. Baek, D. Efremov, J. M. Ok, J. S. Kim, J. van den Brink, and B. Büchner, Nature Materials **14**, 210 (2014).
[6] Y. Su, H. Liao, and T. Li, Journal of Physics: Condensed Matter **27**, 105702 (2015).
[7] S. Mukherjee, A. Kreisel, P. J. Hirschfeld, and B. M. Andersen, Phys. Rev. Lett. **115**, 026402 (2015).
[8] K. Jiang, J. Hu, H. Ding, and Z. Wang, Phys. Rev. B **93**, 115138 (2016).
[9] L. Fanfarillo, G. Giovannetti, M. Capone, and E. Bascones, Phys. Rev. B **95**, 144511 (2017).
[10] R.-Q. Xing, L. Classen, M. Khodas, and A. V. Chubukov, Phys. Rev. B **95**, 085108 (2017).
[11] Q. Wang et al., Nature Materials **15**, 159 (2016).
[12] M. C. Rahn et al., Phys. Rev. B **91**, 180501 (2015).
[13] L. Fanfarillo, A. Cortijo, and B. Valenzuela, Phys. Rev. B **91**, 214515 (2015).
[14] M. H. Christensen, J. Kang, B. M. Andersen, and R. M. Fernandes, Phys. Rev. B **93**, 085136 (2016).
[15] R. Fernandes and C. A., Rep. Prog. Phys. **80**, 014503 (2017).
[16] S. Onari, Y. Yamakawa, and H. Kontani, Phys. Rev. Lett. **116**, 227001 (2016).
[17] J. K. Glasbrenner, I. I. Mazin, H. O. Jeschke, P. J. Hirschfeld, R. M. Fernandes, and R. Valenti, Nature Physics **11**, 953 (2015).
[18] L. Fanfarillo, J. Mansart, P. Toulemonde, H. Cercellier, P. Le Fèvre, F. m. c. Bertran, B. Valenzuela, L. Benfatto, and V. Brouet, Phys. Rev. B **94**, 155138 (2016).
[19] A. V. Chubukov, M. Khodas, and R. M. Fernandes, Phys. Rev. X **6**, 041045 (2016).
[20] Y. Yamakawa, S. Onari, and H. Kontani, Phys. Rev. X **6**, 021032 (2016).
[21] Y. Yamakawa and H. Kontani, arXiv:1609.09618 (2016).
[22] J. P. Sun, K. Matsuura, G. Z. Ye, Y. Mizukami, M. Shimozawa, K. Matsubayashi, M. Yamashita, T. Watashige, S. Kasahara, Y. Matsuda, et al., Nature Communications **7**, 12146 (2016).
[23] K. Kothapalli, A. E. Böhmer, W. T. Jayasekara, B. G. Ueland, P. Das, A. Sapkota, V. Taufour, Y. Xiao, E. Alp, S. L. Budko, et al., Nature Communications **7**, 12728 (2016).
[24] A. I. Coldea and M. D. Watson, ArXiv e-prints (2017), 1706.00338.
[25] M. Khodas and A. Levchenko, Phys. Rev. B **91**, 235119 (2015).
[26] M. H. Christensen, J. Kang, B. M. Andersen, I. Eremin, and R. M. Fernandes, Phys. Rev. B **92**, 214509 (2015).
[27] L. Classen, R.-Q. Xing, M. Khodas, and A. V. Chubukov, Phys. Rev. Lett. **118**, 037001 (2017).
[28] Y. Ran, F. Wang, H. Zhai, A. Vishwanath, and D.-H. Lee, Phys. Rev. B **79**, 014505 (2009).
[29] K. Kuroki, H. Usui, S. Onari, R. Arita, and H. Aoki, Phys. Rev. B **79**, 224511 (2009).
[30] S. Graser, T. Maier, P. Hirschfeld, and D. Scalapino, New J. Phys. **11**, 025016 (2009).
[31] A. F. Kemper, M. M. Korshunov, T. P. Devereaux, J. N. Fry, H.-P. Cheng, and P. J. Hirschfeld, Phys. Rev. B **83**, 184516 (2011).
[32] E. Bascones, B. Valenzuela, and M. J. Calderón, Comptes Rendus Physique **17**, 36 (2016), ISSN 1631-0705.
[33] V. Cvetkovic and O. Vafek, Phys. Rev. B **88**, 134510 (2013).
[34] J. Fink, A. Charnukha, E. D. L. Rienks, Z. H. Liu, S. Thirupathaiah, I. Avigo, F. Roth, H. S. Jeevan, P. Gegenwart, M. Roslova, et al., Phys. Rev. B **92**, 201106 (2015).
[35] J. Fink, E. D. L. Rienks, S. Thirupathaiah, J. Nayak, A. van Roekeghem, S. Biermann, T. Wolf, P. Adelmann, H. S. Jeevan, P. Gegenwart, et al., Phys. Rev. B **95**, 144513 (2017).
[36] I. Avigo, S. Thirupathaiah, E. D. L. Rienks, L. Rettig, A. Charnukha, M. Ligges, R. Cortes, J. Nayak, H. S. Jeevan, T. Wolf, et al., physica status solidi (b) **254**, 1600382 (2017).
[37] See supplemental material.
[38] H. Ding, P. Richard, K. Nakayama, T. Sugawara, T. Arakane, Y. Sekiba, A. Takayama, S. Souma, T. Sato, T. Takahashi, et al., EPL **83**, 47001 (2008).
[39] N.-L. Wang, H. Hosono, and P. Dai, Iron based superconductors (Pan Stanford Publishing, United States, 2013).
[40] R. M. Fernandes and J. Schmalian, Supercond. Sci. Technol. **25**, 084005 (2012).
[41] I. Paul, Phys. Rev. B **90**, 115102 (2014).
[42] P. Reiss, M. D. Watson, T. K. Kim, A. A. Haghighirad, D. N. Woodruff, M. Bruma, S. J. Clarke, and A. I. Coldea, ArXiv e-prints (2017), 1705.11139.
[43] R. Valenti, private communication (2017).
[44] A. Larkin and A. Varlamov, Theory of Fluctuations in Superconductors (Clarendon Press, Oxford, 2005).

[45] D. Inosov, J. Park, P. Bourges, D. L. Sun, Y. Sidis, A. Schneidewind, K. Hradil, D. Haug, C. Lin, B. Keimer, et al., Nature Physics **6**, 178 (2010).
[46] J. Paglione and R. Greene, Nature Physics **6**, 645 (2010).

Supplementary Material for Orbital mismatch boosting nematic instability in iron-based superconductors

In this supplemental material we discuss how to compute the quadratic and quartic coefficients of the action and show the explicit results for the cases of interest. We start from Eq.s (7)-(11) of the main text, that we rewrite here for convenience:

$$\Pi_X^{yz} = T\sum_{\mathbf{k},i\omega_n} u_\Gamma^2 u_X^2 g_+ g_X + v_\Gamma^2 u_X^2 g_- g_X, \quad (18)$$

$$\Pi_Y^{xz} = T\sum_{\mathbf{k},i\omega_n} v_\Gamma^2 u_Y^2 g_+ g_Y + u_\Gamma^2 u_Y^2 g_- g_Y. \quad (19)$$

and

$$u_{11} = T\sum_{\mathbf{k},i\omega_n} (u_X^2 g_X)^2 (u_\Gamma^2 g_+ + v_\Gamma^2 g_-)^2, \quad (20)$$

$$u_{22} = T\sum_{\mathbf{k},i\omega_n} (u_Y^2 g_Y)^2 (v_\Gamma^2 g_+ + u_\Gamma^2 g_-)^2, \quad (21)$$

$$u_{12} = T\sum_{\mathbf{k},i\omega_n} u_X^2 g_X u_Y^2 g_Y u_\Gamma^2 v_\Gamma^2 (g_+ - g_-)^2. \quad (22)$$

As already discussed the quartic part of the action can be simply diagonalized as $S_{\rm eff}^{(4)} = \lambda_\psi \psi^2 + \lambda_\phi \phi^2$ with

$$\psi = \frac{1}{\sqrt{2}}(\Delta_X^{yz})^2 + (\Delta_Y^{xz})^2, \quad \lambda_\psi = u_{11} + u_{12} \quad (23)$$

$$\phi = \frac{1}{\sqrt{2}}(\Delta_X^{yz})^2 - (\Delta_Y^{xz})^2, \quad \lambda_\phi = u_{11} - u_{12}, \quad (24)$$

where we used that $u_{11} = u_{22}$. An attractive nematic coupling $\lambda_\phi < 0$ is a necessary (but not sufficient) condition for the occurrence of the nematic transition, that happens only if a divergence of the susceptibility χ_{nem} is found at a nematic critical temperature T_{nem}.

GREEN FUNCTIONS WITHIN THE PERFECTLY NESTED PARABOLIC BAND APPROXIMATION AND BEYOND

To make a first estimate of Eq.s (18)-(22) we consider the simple case where the electron/hole pockets are perfectly nested circular Fermi surfaces. The orbital weights simply become:

$$u_\Gamma = u_Y = v_X = \cos\theta_{\mathbf{k}}, \quad v_\Gamma = v_Y = u_X = \sin\theta_{\mathbf{k}} \quad (25)$$

with $\theta_{\mathbf{k}} = \arctan(k_y/k_x)$. One can also put $g_X = g_Y = g_e = (i\omega_n - \epsilon)^{-1}$ while $g_+ = g_- = g_h = (i\omega_n + \epsilon)^{-1}$. Here ϵ is the parabolic dispersion $\epsilon = -\epsilon_0 + \mathbf{k}^2/2m$, with ϵ_0 is the off-set energy with respect to the chemical potential, put conventionally to zero, and m the parabolic band mass.

As mentioned in the manuscript, we account for the deviations from the perfectly-nested parabolic-band approximation perturbatively. One can describe the ellipticity of the electronic band dispersion as

$$E^{X/Y} \simeq \epsilon \mp \delta_e \cos 2\theta_{\mathbf{k}}, \qquad \delta_e = \epsilon_0\, m\,(\frac{m_x - m_y}{2m_x m_y}), \quad (26)$$

where δ_e accounts for the ellipticity of the electron pocket via the x/y anisotropy of the masses with respect the parabolic band mass m. The expressions in Eq.s (26) correctly reproduces the opposite ellipticity of the X/Y pockets. For the sake of completeness we also consider the deviation from perfect nesting due to e.g. mass, offset energy, spin-orbit coupling mismatch of the hole pockets via

$$E^{\Gamma_\pm} \simeq -\epsilon + \delta_{m_\pm}, \qquad \delta_{m_\pm} = \epsilon_0\left(\frac{m_\pm - m}{m}\right). \quad (27)$$

These perturbations can be included in the estimate of Eqs.(18)-(22) by expanding the Green functions for small δ_e, $\delta_{m_\pm}$:

$$g_\pm = g_h(1 + \delta_{m_\pm} g_h) \quad (28)$$

$$g_{X/Y} = g_e(1 \mp \delta_e \cos(2\theta_{\mathbf{k}}) g_e). \quad (29)$$

In principle the perturbations δ_e and $\delta_{m_\pm}$ affect also the angular orbital factors, which should deviate from the $\cos\theta/\sin\theta$ expressions of Eq.(25). However in first approximation we will neglect these modifications and we will retain only the effects of δ_e and $\delta_{m_\pm}$ on the Green's functions.

EVALUATION OF THE SUM OVER FREQUENCY AND MOMENTA

To compute the sum over Matsubara frequency and momenta in Eq.s (18)-(22) we will use the usual decomposition:

$$\sum_{\mathbf{k}} = \int_{BZ} \frac{d^2\mathbf{k}}{(2\pi)^2} = \int_0^{2\pi} \frac{d\theta}{2\pi} \int d\epsilon N_F \quad (30)$$

where ϵ is the energy, θ the azimuthal angle $N_F = m/2\pi$ is the density of state per spin at the Fermi level in 2D. In this way the only difference between the various models is in the angular integration of the orbital factors. Let us then discuss briefly the remaining common integrals over energy and the Matsubara sums.

Starting from the Gaussian term within the perfectly nested parabolic band approximation we need to compute the Π_{eh} bubble

$$\Pi_{eh} \equiv T N_F \sum_{i\omega_n} \int d\epsilon \, g_e g_h \tag{31}$$

By performing the energy integration via the calculus of the residua of the Green functions' poles we found

$$\Pi_{eh} = -2N_F T \sum_{n\geq 0} \frac{\pi}{\omega_n} = -N_F \sum_{n\geq 0} \frac{1}{(n+1/2)} \tag{32}$$

where we used that $\omega_n = 2\pi T(n+1/2)$. The calculation of the above sum can be carried out in terms of Euler digamma functions [44].

$$\psi^{(N)}(z) = (-1)^{N+1} N! \sum_{n=0}^{\infty} \frac{1}{(n+z)^{N+1}}. \tag{33}$$

The logarithmic divergence at the upper limit ($\psi^{(0)}(z >> 1) \sim ln(z)$) is cut-off by the ω_0 typical energy scale of the spin mode and one gets

$$\begin{aligned} \Pi_{eh} &= -N_F \left(\psi^{(0)}\left(\frac{1}{2} + \frac{\omega_0}{2\pi T}\right) - \psi^{(0)}\left(\frac{1}{2}\right)\right) \\ &= -N_F \Big(ln(\omega_0/T) + ln(2/\pi) + C_E \Big) \end{aligned} \tag{34}$$

where we used that $\psi^{(0)}(1/2) = -C_E - 2ln(2)$ with C_E being the Euler-Mascheroni constant.

In order to compute the quartic terms, Eq.s (20)-(22), within the perfectly nested parabolic band approximation we need to compute

$$T \sum_{i\omega_n} \int d\epsilon \, g_e^2 g_h^2 = T \sum_{n\geq 0} \frac{\pi}{{\omega_n}^3} \tag{35}$$

while beyond such approximation the Green functions expansion lead to:

$$\begin{aligned} T \sum_{i\omega_n} \int d\epsilon \, g_e^4 g_h^2 &= -T \sum_{n\geq 0} \frac{\pi}{2\,{\omega_n}^5} \\ T \sum_{i\omega_n} \int d\epsilon \, g_e^3 g_h^3 &= -T \sum_{n\geq 0} \frac{3\,\pi}{4\,{\omega_n}^5} \end{aligned} \tag{36}$$

and analogously for the $g_e^2 g_h^4$ case. It is easy to verify that the integrals of combination $(g_e g_h)^{m_1} g_{e/h}^{2m_2+1}$ with odd unpaired powers of the e/h Green's functions vanish, since the contribution coming from Matsubara frequency with positive n exactly cancels out with the contribution of the negative ones. Using that $\omega_n = 2\pi T(n+1/2)$, one can recognize in Eq.s (35)-(36) the Euler digamma functions, Eq.(33) for $z = 1/2$ and $N = 2, 4$ [44]. For $z = 1/2$ one can express $\psi^{(N)}(1/2)$ in terms of the Riemann $\zeta(n)$ functions as

$$\psi^{(N)}(1/2) = (-1)^{N+1} N! \, (2^{N+1} - 1)\zeta(N+1)$$

Using these definitions in Eq.s (35)-(36) we obtain

$$T \sum_{i\omega_n} \int d\epsilon \, g_e^2 g_h^2 = \frac{7\zeta(3)}{8\pi^2 T^2} \equiv \mathcal{A}(T) \tag{37}$$

$$T \sum_{i\omega_n} \int d\epsilon \, g_e^4 g_h^2 = -\frac{31\zeta(5)}{64\pi^4 T^4} \equiv \mathcal{B}(T) \tag{38}$$

$$T \sum_{i\omega_n} \int d\epsilon \, g_e^3 g_h^3 = -\frac{93\,\zeta(5)}{128\pi^4 T^4} \equiv \mathcal{C}(T) \tag{39}$$

where $\zeta(3) \sim 1.202$ and $\zeta(5) \sim 1.037$, from which it follows that

$$\mathcal{B}(T) = -\frac{b\,\mathcal{A}(T)}{T^2} \qquad \mathcal{C}(T) = -\frac{3\,b\mathcal{A}(T)}{2\,T^2} \tag{40}$$

with $b \sim 0.048$.

ESTIMATE OF THE QUADRATIC AND QUARTIC TERMS OF THE ACTION

3-pocket model $\Gamma_+ XY$: complete orbital mismatch

In this case we need to account only for the contribution coming from the Γ_+ in Eq.s (18)-(22). The quadratic term in the $q = 0$ limit is given by

$$\begin{aligned} \Pi_{X/Y}^{yz/xz} &= T \sum_{\mathbf{k}, i\omega_n} g_h g_e \sin^2\cos^2\theta = \frac{\Pi_{eh}}{8} \\ &= -\frac{N_F}{8}\Big(\ln(\omega_0/T) + const \Big) \end{aligned} \tag{41}$$

with $const = ln(2/\pi) + C_E$. Here we separated the integrations as in Eq.(30), used the results of Eq.(34) and performed the angular integral $\int (d\theta/2\pi) \sin^2\theta \cos^2\theta = 1/8$. The Neél temperature is determined as the temperature at which the pole of the magnetic susceptibility occurs

$${\chi_{X/Y}^{yz/xz}}^{-1}(q=0) = \frac{1}{U_s} + \Pi_{X/Y}^{yz/xz} = \frac{N_F}{8} \ln\left(\frac{T}{T_{Neel}}\right) \tag{42}$$

where

$$T_{Neel} = 1.13\,\omega_0\, e^{-8/(N_F\, U_S)}. \tag{43}$$

Concerning the quartic term, we have that within the perfectly-nested parabolic-band approximation all the quartic coefficients, Eq.s (20)-(22), are equivalent $u^0_{11/22} = u^0_{12} = u^0$

$$u^0 = T \sum_{\mathbf{k}, i\omega_n} g_h^2\, g_e^2 \sin^4\theta \cos^4\theta = \frac{3\,N_F}{128} \mathcal{A}(T) \tag{44}$$

where we borrowed the results from Eq. (37) and computed the angular integral. In this case from the diagonalization of the quartic form, Eq.s (23)-(24), we obtain

$$\lambda^0_\psi = \frac{3\,N_F}{64} \mathcal{A}(T) \qquad \lambda^0_\phi = 0 \tag{45}$$

Beyond the perfectly-nested parabolic-band approximation we can include the effects of the band nesting mismatch of the Γ_+ pocket and of the ellipticity of the electron pocket using the Green functions' expansion of Eq.s (28)-(29). With simple steps by using the integrals Eq.s (37)-(38) one can easily obtain the expressions for the u_{ij} terms up to order δ_e^2, $\delta_{m_\pm}^2$

$$u_{11/12} = \frac{N_F\,\mathcal{A}(T)}{128}\left[3 - \frac{b}{T^2}\left(3\delta_{m_+}^2 \pm \frac{1}{2}\delta_e^2\right)\right] \qquad (46)$$

where we further simplified our expressions accounting for the relation between $\mathcal{A}(T)$ and $\mathcal{B}(T)$ (see Eq. (40)). It is now straightforward to compute the $\lambda_{\psi/\phi}$ coupling

$$\lambda_\psi = \frac{3\,N_F\,\mathcal{A}(T)}{64}\left(1 - \frac{b}{T^2}\delta_{m_+}^2\right) \qquad (47)$$

$$\lambda_\phi = -\frac{N_F\,\mathcal{A}(T)}{64}\frac{b}{T^2}\delta_e^2 \qquad (48)$$

as quoted in the main manuscript, with the definition $\mathcal{K}(T) = N_F\mathcal{A}(T)/64$.

3-pocket model $\Gamma_- XY$: the perfect orbital match

We proceed in analogous way to compute the quadratic and quartic coefficients for the other cases of interest. Within a 3-pocket model $\Gamma_- XY$ we account for the contribution of the Γ_- pocket only. The quadratic term in the $q = 0$ limit in this case is given by

$$\Pi_X^{yz} = T\sum_{\mathbf{k},i\omega_n} g_h g_e \sin^4\theta = \frac{3}{8}\Pi_{eh} = -\frac{3N_F}{8}\left(\ln(\omega_0/T) + const\right) \qquad (49)$$

where we used $\int (d\theta/2\pi)\sin^4\theta = 3/8$. As expected the same result is found for Π_Y^{xz} where the angular factor goes like $\int (d\theta/2\pi)\cos^4\theta = 3/8$. The magnetic susceptibility is given by

$$\chi_{X/Y}^{yz/xz\,-1}(q=0) = \frac{3N_F}{8}\ln\left(\frac{T}{T_{Neel}}\right) \qquad (50)$$

and the Neél temperature is

$$T_{Neel} = 1.13\,\omega_0\,e^{-8/(3\,N_F\,U_S)}. \qquad (51)$$

Concerning the quartic coefficients, within the perfectly-nested parabolic-band approximation, we have

$$u_{11/22}^0 = T\sum_{\mathbf{k},i\omega_n} g_h^2\,g_e^2\sin^4\theta\sin^4\theta = \frac{35\,N_F}{128}\mathcal{A}(T)$$

$$u_{12}^0 = T\sum_{\mathbf{k},i\omega_n} g_h^2\,g_e^2\sin^4\theta\cos^4\theta = \frac{3\,N_F}{128}\mathcal{A}(T) \qquad (52)$$

Since now $u_{11/22} \neq u_{12}$ the diagonalization of the quartic form Eq.s (23)-(24) lead to a finite λ_ϕ^0

$$\lambda_\psi^0 = \frac{19\,N_F}{64}\mathcal{A}(T) \qquad \lambda_\phi^0 = \frac{16\,N_F}{64}\mathcal{A}(T) \qquad (53)$$

The contributions coming from the next orders δ_e, δ_{m_-} can be computed following the same approach used in the previous section. Through tedious but straightforward calculations, using Eq.s (37)-(39) for computing the integrals and the relations among $\mathcal{A}(T)$, $\mathcal{B}(T)$ and $\mathcal{C}(T)$ of Eq. (40), one arrives at

$$\lambda_\psi = \frac{N_F\,\mathcal{A}(T)}{128}\left(38 - \frac{b}{T^2}\left(38\delta_{m_-}^2 + 24\delta_e^2 + 168\delta_e\delta_{m_-}\right)\right)$$

$$\lambda_\phi = \frac{N_F\,\mathcal{A}(T)}{128}\left(32 - \frac{b}{T^2}\left(32\delta_{m_-}^2 + 25\delta_e^2 + 168\delta_e\delta_{m_-}\right)\right). \qquad (54)$$

that in the limit $\delta_{m_-} \to 0$ reduce to the expressions quoted in the main manuscript.

4-pocket: $\Gamma_\pm, X, Y$

Within the 4-pocket model both the outer and inner hole pockets contribute to the quadratic and quartic coefficients of the action Eq.s (18)-(22). The quadratic term in the $q = 0$ limit in this case is given by

$$\Pi_X^{yz} = T\sum_{\mathbf{k},i\omega_n} g_h g_e(\cos^2\theta\sin^2\theta + \sin^4\theta) = \frac{\Pi_{eh}}{2} = -\frac{N_F}{2}\left(\ln(\omega_0/T) + const\right) \qquad (55)$$

and analogous for Π_Y^{xz}. The magnetic susceptibility is given by

$$\chi_{X/Y}^{yz/xz\,-1}(q=0) = \frac{N_F}{2}\ln\left(\frac{T}{T_{Neel}}\right) \qquad (56)$$

where the Neél temperature is

$$T_{Neel} = 1.13\,\omega_0\,e^{-2/(N_F\,U_S)}. \qquad (57)$$

Within the perfectly-nested parabolic-band approximation the quartic coefficients go as

$$u_{11}^0 = T\sum_{\mathbf{k},i\omega_n} g_h^2\,g_e^2\sin^4\theta = \frac{3\,N_F}{8}\mathcal{A}(T)$$

$$u_{22}^0 = T\sum_{\mathbf{k},i\omega_n} g_h^2\,g_e^2\cos^4\theta = \frac{3\,N_F}{8}\mathcal{A}(T)$$

$$u_{12}^0 = T\sum_{\mathbf{k},i\omega_n} g_e^2(g_h - g_h)^2\sin^4\theta\cos^4\theta = 0 \qquad (58)$$

Since here $u_{12} = 0$ from Eq.s (23)-(24) we find two identical coupling at the lower order

$$\lambda_\psi^0 = \lambda_\phi^0 = \frac{3\,N_F}{8}\mathcal{A}(T) \qquad (59)$$

The effect of the perturbations δ_e, δ_{m_-} can be computed as before and contributes to the $\lambda_{\psi/\phi}$ couplings as

$$\lambda_\psi = \frac{N_F\,\mathcal{A}(T)}{64}\left(24 - \frac{b}{T^2}\left(19\delta_{m_-}^2 + 14\delta_e^2 + 90\delta_e\delta_{m_-}\right)\right)$$
$$\lambda_\phi = \frac{N_F\,\mathcal{A}(T)}{64}\left(24 - \frac{b}{T^2}\left(16\delta_{m_-}^2 + 14\delta_e^2 + 90\delta_e\delta_{m_-}\right)\right). \quad (60)$$

QUANTITATIVE ANALYSIS OF THE RESULTS FOR THE 3-POCKET, Γ_+XY, Γ_-XY, AND 4-POCKET, $\Gamma_\pm XY$, MODELS

To elucidate the effects of the orbital mismatch on suppressing magnetism and boosting nematicity, we will consider band-structure parameters appropriate for 122 iron-based compounds e.g. $BaFe_2As_2$. For the spin fluctuations we refer to [45] and use $\omega_0 \sim 18$ meV.

We first consider the difference in Neél temperatures, T_{Neel}, for the two the 3-pocket models, Γ_+XY ($3p_+$) and Γ_-XY ($3p_-$). To determine T_{Neel} we need the value of the low-energy coupling U_s. We choose this value in order to reproduce, within the Γ_-XY model, the experimental value $T_{Neel} \sim 110$ K found for weakly doped $BaFe_2As_2$ compounds [46]. Keeping then all the parameters fixed we can estimate the value of T_{Neel} in the Γ_+XY model, which only differs in the orbital composition of the hole pocket at Γ. From Eq. (43) we then obtain $T_{Neel} = 24$ K, i.e. a suppression of the $\sim 80\%$ with respect the Γ_-XY model, uniquely due to the different degree of orbital matching between hole and electron pockets of the two cases. A more precise estimate for FeSe would require to account also for the different band-structure parameters in the two cases. In particular FeSe is characterized by electron pockets with a density of states N_F about 30% smaller than in 122 compounds [18]. If we account for this difference in Eq. (43) the T_{Neel} of the Γ_+XY model, used to describe FeSe, is further suppressed, approaching the critical temperature of the superconducting instability of FeSe.

For sake of completeness we also compute T_{Neel} for the 4-pocket model from Eq. (57). In this case, since both the inner and outer pockets $\Gamma_\pm$ contribute to the instability, the Neél temperature reaches the 130 K.

Once computed the Neél temperature for the various cases (TABLE: I), we can easily compute the $q = 0$ magnetic susceptibility as in Eq.s (42), (50), (56). We show in Fig. 3a of the main text the temperature dependence of the susceptibility $\chi = \chi^{yz/xz}_{X/Y}$ for the $3p_-$ /$3p_+$ models using $T_{Neel} = 110/24$ K respectively. The density of states $N_F \sim 1.3$ eV^{-1} is derived assuming $1/(2m) \sim 60$ meV. The typical logarithmical divergence is found at the correspondent T_{Neel}. It is interesting to notice that due to the different numerical prefactors (1/8 vs 3/8) in Eq.s (42) and (50) $\chi(q = 0)$ takes similar value for the two model around room temperature even if the divergence of the χ_{3p_+} is found at lower temperature with respect to the $3p_-$ case.

Model:	$3p_+$ (FeSe)	$3p_-$	4p
T_{Neel} (K)	24	110	132

TABLE I: T_{Neel} for the 3-pocket models, Γ_+XY ($3p_+$) and Γ_-XY ($3p_-$), and for the 4-pocket model $\Gamma_\pm XY$ (4p). Assuming $T_{Neel} \sim 110$ K for the $3p_-$ model we estimate $N_F U_s$ and use this values to compute the Neel temperature of the other cases. For the $3p_+$ model we find a suppression of the 80% with respect the $3p_-$ case due to the orbital mismatch. In FeSe we expect an even stronger suppression since its experimental density of states is lower than in the 122 family. A higher T_{Neel} is found instead in the 4p model, in which both the inner and outer hole pockets contribute to the magnetic instability.

Concerning the quartic-order coefficients of the action, a qualitative analysis of Eq.s (47)-(48), (54) and (60) shows that:

(i) For the $3p_+$ model (FeSe case) independently on others parameters the nematic coupling λ_ϕ Eq. (48) is negative as soon as the ellipticity of the electron pockets is considered, while the symmetric eigenvalue λ_ψ Eq. (47) remains finite and positive.

(ii) For the $3p_-$ model, as one can check from Eq. (54), at any value of δ_{m_-} the first eigenvalue which becomes negative for decreasing temperature is λ_ϕ. Thus the ellipticity is again the driving force for the nematic transition. However here we need a finite value of δ_e in order to induce a sign change in λ_ϕ. Putting $\delta_{m_-} = 0$ one can derive the temperature T^* below which the nematic eigenvalue becomes negative as a function δ_e, $T^* = (25\,b/32)^{1/2}\delta_e \sim 0.19\ \delta_e$

(iii) For the complete 4p model a nematic instability is prevented by the sign of the nematic eigenvalue (see Eq. (60)). Indeed in this case at any finite value of δ_{m_-} the first eigenvalue which becomes negative for decreasing temperature is λ_ψ. Assuming $\delta_{m_-} = 0$ the correction to λ_ψ and λ_ϕ reduces to the identical δ_e^2 term thus the temperature T^* below which the nematic eigenvalue becomes negative is, as a matter of fact, the same that determines the change of sign of λ_ψ.

Finally, we need to choose some parameter values for a quantitative estimate of the nematic coupling of the 3 pocket models used in Fig. 3b of the main text. For

BAND Parameters	
ϵ_0 (meV)	90
$1/(2m)$ (meV)	60
N_F (ev^{-1})	1.3
k_F^0 (π/a)	0.31
δ_e/ϵ_0	0.55
k_{Fx} (π/a)	0.39
k_{Fy} (π/a)	0.21

TABLE II: Band parameters appropriate for 122 compounds used in this section.

the band structure we choose again parameters appropriate for weakly-doped 122 compounds: we set $\epsilon_0 = 90$ meV and $1/(2m) \sim 60$ meV, ($N_F \sim 1.3$ eV^{-1}). With these parameters we have circular Fermi pockets of radius $k_F^0 \sim 0.31$ in π/a unit, $a \sim 3.96$ Å is the lattice parameter. Beyond the parabolic-band approximation we further consider the ellipticity of the electron pockets Eq. (26) assuming $\delta_e = 0.55\epsilon_0$. This define electronic elliptical Fermi pockets with $k_F^{x/y} \sim 0.39$ and $k_F^{y/x} \sim 0.21$ for the X/Y pockets respectively. For simplicity we consider the case $\delta_{m_-} = 0$. Any finite value of such a perturbation lead to similar conclusions. All the band parameters used are collected in TABLE: II. The nematic eigenvalue λ_ϕ for the $3p_+$ model Eq. (48) and for the $3p_-$ model Eq. (54) as a function of T are plotted in Fig. 3b in the main text. While for the $3p_+$ case the nematic coupling is negative at any temperature, for the $3p_-$ model we need to cool the system below $T^* \sim 112$ K in order induce a sign change in the nematic eigenvalue. Below this temperature the absolute value of λ_ϕ grows rapidly with decreasing T, explaining why in this system, where $T_{Neel} = 110$ K, the nematic transition occurs very close to the magnetic one. Notice that the relative value of T^* and T_{Neel} can slightly vary in different 122 compounds and different doping level depending on the band parameters. In particular for small δ_e, T^* can be even lower than T_{Neel} preventing the occurrence of a nematic phase.